A WENO-solver for the 1D non-stationary Boltzmann–Poisson system for semiconductor devices

José A. Carrillo*, Irene M. Gamba†, Armando Majorana‡ and Chi-Wang Shu§

October 12, 2001

Abstract

In this work we present preliminary results of a high order WENO scheme applied to a new formulation of the Boltzmann equation (BTE) describing electron transport in semiconductor devices with a spherical coordinate system for the phase velocity space. The problem is two dimensional in the phase velocity space and one dimensional in the physical space, plus the time variable driving to steady states. The new formulation avoids the singularity due to the spherical coordinate system.

Keywords: Boltzmann equation for semiconductors, WENO scheme, spherical coordinate system.

*Departamento de Matemática Aplicada, Universidad de Granada, 18071 Granada, Spain. E-mail: carrillo@ugr.es. Research of this author is supported by the spanish DGES project PB98-1281 and the TMR Project "Asymptotic Methods in Kinetic Theory" ERB-FRMXCT-970157.

†Department of Mathematics, University of Texas at Austin, USA. E-mail: gamba@math.utexas.edu. Research of this author is supported by NSF under grant DMS 9971779 and TARP 003658-0459-1999.

‡Dipartimento di Matematica e Informatica, Universita' di Catania, Catania, Italy. E-mail: majorana@dmi.unict.it. Research of this author is supported by C.N.R. contributo N.98.03630.ST74 and the TMR Project "Asymptotic Methods in Kinetic Theory" ERB-FRMXCT-970157.

§Division of Applied Mathematics, Brown University, Providence, RI 02912, USA. e-mail: shu@cfm.brown.edu. Phone: 1-401-863-2549. FAX: 1-401-863-1355. To whom correspondence should be sent. Research of this author is supported by NSF grant ECS-9906606 and ARO grant DAAD19-00-1-0405.

1 Introduction

The Boltzmann equation (BTE) describes electron transport in semiconductor devices. Solving it numerically is not an easy task because the BTE is an integro-differential equation with six dimensions (three in the phase velocity space and three in the physical space) and one additional dimension in time. Actually, one of the most popular method to model charge transport in such devices is the Monte Carlo method. However, it could be very noisy at extreme regimes. Fatemi and Odeh [1] developed a finite difference scheme for solving the Boltzmann-Poisson system. They used a spherical coordinate system for the phase velocity space and a first order upwind scheme to discretize the differential terms in the BTE. However, their approach introduces a singularity in the free streaming operator, the treatment of which in [1] is ad hoc.

Recently Majorana and Pidatella [3] introduced a new solver for the BTE based on the finite difference box method. A new formulation is introduced to avoid the above singularity. In this paper, we apply the high order non-oscillatory finite difference WENO schemes [2] to this formulation, resulting in a solver which is high order accurate regardless of the irregularity of the distribution function near the junctions of the device. Preliminary numerical results are shown to demonstrate the capability of this solver.

2 Basic equations

We consider an electron gas, which interacts with a bath of phonons assumed to be in thermal equilibrium. In this case the Boltzmann equation is

$$\frac{\partial f}{\partial t} + \frac{1}{\hbar}\nabla_{\mathsf{k}}\varepsilon \cdot \nabla_{\mathsf{x}} f - \frac{\mathfrak{e}}{\hbar}\mathsf{E} \cdot \nabla_{\mathsf{k}} f = Q(f). \tag{2.1}$$

The unknown f is the electron distribution function, which depends on time t, space coordinates x and phase velocity vector k. The parameters $\hbar$ and $\mathfrak{e}$ are the Planck constant divided by 2π and the positive electric charge, respectively. The symbol ∇_{k} stands for the gradient with respect to the variables k and ∇_{x} that with respect to the space coordinates

x. The particle energy ε is an assigned nonnegative continuous function. If the Kane model is assumed, then

$$\varepsilon(\mathsf{k}) = \frac{1}{1+\sqrt{1+2\,\dfrac{\tilde{\alpha}}{m^*}\hbar^2\,|\mathsf{k}|^2}}\frac{\hbar^2}{m^*}\,|\mathsf{k}|^2\,, \tag{2.2}$$

where m^* is the effective mass and $\tilde{\alpha}$ is the nonparabolicity factor. The widely used parabolic approximation is obtained from Eq. (2.2) by putting $\tilde{\alpha}=0$.

In Eq. (2.1) the electric field E satisfies the Poisson equation

$$\Delta V = \frac{\mathfrak{e}}{\epsilon}\left[n(t,\mathsf{x}) - N_D(\mathsf{x})\right], \tag{2.3}$$

$$\mathsf{E} = -\nabla_{\mathsf{x}} V, \tag{2.4}$$

where ϵ is the permittivity, $n(t,\mathsf{x}) = \int_{\Re^3} f(t,\mathsf{x},\mathsf{k})\,d\mathsf{k}$ is the electron density, $N_D(\mathsf{x})$ is the doping and V is the electric potential. Eqs. (2.1)-(2.3)-(2.4) give the Boltzmann-Poisson system.

We follow a semi-classical approach for the collision term $Q(f)$, so that, in the low density regime, it is

$$Q(f)(t,\mathsf{x},\mathsf{k}) = \int_{\mathbb{R}^3}\left[S(\mathsf{k}',\mathsf{k})f(t,\mathsf{x},\mathsf{k}') - S(\mathsf{k},\mathsf{k}')f(t,\mathsf{x},\mathsf{k})\right]\,d\mathsf{k}'\,. \tag{2.5}$$

The kernel S, which takes into account the scattering processes between electrons and phonons, is defined by

$$\begin{aligned} S(\mathsf{k},\mathsf{k}') &= K_0(\mathsf{k},\mathsf{k}')\delta(\varepsilon(\mathsf{k}')-\varepsilon(\mathsf{k})) + K(\mathsf{k},\mathsf{k}') \\ &\times\left[(\mathsf{n}_q+1)\,\delta(\varepsilon(\mathsf{k}')-\varepsilon(\mathsf{k})+\hbar\omega) + \mathsf{n}_q\delta(\varepsilon(\mathsf{k}')-\varepsilon(\mathsf{k})-\hbar\omega)\right]\,. \end{aligned} \tag{2.6}$$

Here, we have included intra-valley acoustic phonon scattering in the elastic approximation and intra-valley optical non-polar phonon scattering with one frequency. These scattering mechanisms are chosen because of their importance in Si. The constant n_q is the occupation number of phonons and is given by

$$\mathsf{n}_q = \left[\exp\left(\frac{\hbar\omega}{k_B T_L}\right) - 1\right]^{-1}\,,$$

where ω is the constant phonon frequency, k_B is the Boltzmann constant and T_L is the lattice temperature. The symbol δ indicates the usual Dirac distribution.

We are looking for a solution of the BTE, which depends only on one spatial coordinate, denoted by z. It is useful to introduce dimensionless equations, and to use the following coordinate transformation

$$\mathsf{k} = \sqrt{2}\frac{\sqrt{m^* k_B T_L}}{\hbar}\sqrt{w}\sqrt{1+\alpha_K w}\,(\sqrt{1-\mu^2}\cos\phi, \sqrt{1-\mu^2}\sin\phi, \mu) \tag{2.7}$$

where $\alpha_K = k_B T_L \tilde{\alpha}$ and w is a dimensionless energy.

Eq. (2.7) is equivalent to the spherical coordinate transformation when the parabolic band approximation is used. The main advantage of the new coordinates is the easy treatment of the δ function. In fact, it is simple to check that

$$\varepsilon = k_B T_L w,$$

so that the integrals with respect to w in the collision operator can be solved exactly by using the properties of the δ function. The use of a new dimensionless unknown Φ instead of the distribution function f allows us to write the Boltzmann equation in the following conservative form:

$$\frac{\partial \Phi}{\partial t} + \frac{\partial}{\partial z}(a_1 \Phi) + \frac{\partial}{\partial w}(a_2 \Phi) + \frac{\partial}{\partial \mu}(a_3 \Phi) = C(\Phi)\,, \tag{2.8}$$

where

$$\Phi(t, z, w, \mu) = s(w) f(t, z, w, \mu)$$

except multiplication of dimensional constants with $s(w) = (1+2\alpha_K w)\sqrt{w(1+\alpha_K w)}$. The functions a_i depend on the variables w, μ and the electric field. The operator C replaces the collision operator $Q(f)$. More precisely after taking suitable dimensionless variables, they are given by

$$a_1 = a_1(w, \mu) = \frac{1}{t_*}\frac{\mu s(w)}{(1+2\alpha_K w)^2},$$

$$a_2 = a_2(t, z, w, \mu) = -\frac{E(t, z)}{t_*}\frac{2\mu s(w)}{(1+2\alpha_K w)^2}$$

and

$$a_3 = a_3(t,z,w,\mu) = -\frac{E(t,z)}{t_*}\frac{(1-\mu^2)(1+2\alpha_K w)}{s(w)}.$$

The new collision operator is given by mere evaluations and one dimensional integrals of the new unknown Φ:

$$C(\Phi)(\mathsf{k}) = \frac{s(w)}{t_*}\left\{\frac{1}{2}\int_{-1}^{1}[\beta\Phi(t,z,w,\mu') + a\Phi(t,z,w+\alpha,\mu') + \Phi(t,z,w-\alpha,\mu')]d\mu'\right.$$
$$\left. -\frac{1}{s(w)}[\beta s(w) + as(w-\alpha) + s(w+\alpha)]\Phi(t,z,w,\mu)\right\},$$

where t_*, α and β depend on the physical constants in the scattering mechanisms. Let us remark that the flux coefficients a_1 and a_2 are completely smooth in the variables w and μ, assuming E is smooth. The flux coefficient a_3 is singular for zero energy $w = 0$, however when multiplied with Φ it should form a smooth flux as Φ contains a factor $s(w)$ to cancel the denominator in a_3.

3 WENO schemes

We apply the fifth order weighted ENO (WENO) schemes developed in [2] to the conservation law equation (2.8). WENO schemes are designed for hyperbolic conservation laws or other problems containing either discontinuous solutions or solutions with sharp gradients. The guiding principle is an adaptive usage of a nonlinear convex combination of contributions from local stencils, so that contributions from stencils containing a possible discontinuity or other unpleasant features (e.g., a high gradient) are assigned a nearly zero weight (hence the term weighted essentially non-oscillatory, or WENO). In doing this, uniform high order accuracy can be achieved without introducing any oscillations near discontinuities or sharp gradient regions. Steady state is achieved by a time accurate marching, allowing us to use the same code to simulate time accurate solutions. The high order accuracy of these algorithms allows us to use relatively coarse grids and still get very accurate results. The algorithms have been successfully applied to many applications in various areas of computational physics, such as gas dynamics, astrophysics, etc. For a review of these algorithms, we refer to the lecture notes [4].

4 Numerical results

We consider a Si n^+-n-n^+ diode of a total length of $0.25\mu m$, with a $50nm$ channel located in the middle of the device. The dimensional doping is given by $N_D = 5 \times 10^{18} cm^{-3}$ in the n^+ region and $N_D = 10^{18} cm^{-3}$ in the n region. The input parameters are time in picoseconds ps, length in microns μm and V_{bias} in Volt V.

Our computational parameters for the integral operator $C(\Phi)$ are characteristic time $t_* \approx 3.58923$ ps, dimensionless Kane constant $\alpha_K \approx 0.012926$, scattering mechanism constants $\beta \approx 5.986$, $\alpha \approx 2.43694$, $a = \exp(\alpha) \approx 11.438$ and $c_p \approx 1.10822 \times 10^6$ is the dimensionless constant for the rescaled Poisson equation. See [3] for details.

In the following sequel we include the plots of the modified electron distribution function $\Phi(t, z, w, \mu) = s(w) f(t, z, w, \mu)$ of the Kane (non-parabolic band) model, in Figure 1, left, in spherical coordinates for a potential bias of $V_{bias} = 1$V localized at the point $z = z_0 = 0.125\mu m$ in the middle of the channel. A sharp anisotropy can be observed in the angular component μ, with a drifted mode localized at the scale of the mean velocity corresponding at z_0. In addition, the tail is grossly overpopulated with respect to a shifted Maxwellian distribution. The computation corresponds to time $t = 2ps$. Also, our numerical output indicates that the total current (momentum) flux has not stabilized yet near the junctions for that time scale, Figure 1, right. There is a fluctuation up to 7% still unsettled near the left junction. This may indicate more work is needed for the numerical scheme.

Figure 1 should be put here

We also compare the results at the same V_{bias} and spatial localization z_0, for the parabolic band approximation model and their respective momentum, in Figure 2.

Figure 2 should be put here

We compare the IV-curves for the parabolic and non-parabolic (Kane model) band case

for this device for V_{bias} ranging from 0 to 3 V, in Figure 3. Notice that the non-parabolic Kane model produces lower current for the same V_{bias}.

Figure 3 should be put here

Finally we present the comparison of the first thermodynamic quantities of f, namely the concentration n, the mean velocity v, and the kinetic energy W, for both parabolic and non-parabolic (Kane) bands models on this device at $V_{bias} = 1$ V, in Figure 4. The electric field $E = \Phi'(z)$ is also plotted in Figure 4. We can see that the non-parabolic Kane model produces a significantly lower velocity v.

Figure 4 should be put here

5 Conclusions

Our computational method provides a direct deterministic simulation for the electron distribution function that is accurate and considerably more computationally efficient for channel geometries than a Monte Carlo solver. Monte Carlo solver tends to give a more noisy, and not so reliable result for shorter channels that have more singular solutions, and needs more CPU time than our code to get comparable resolution. Also, since our code is time accurate, it can be used to capture transients in time dependent devices.

In our preliminary numerical simulation, we have observed a lower IV curve for the Kane model than for the parabolic band approximation one. Comparisons with Monte Carlo simulations and with various moment models such as hydrodynamic and energy transport models, and experiments on other devices, will be performed in future work.

References

[1] E. Fatemi and F. Odeh, *Upwind finite difference solution of Boltzmann equation applied to electron transport in semiconductor devices*, J. Comput. Phys. **108**, 1993, pp.209–217.

[2] G. Jiang and C.-W. Shu, *Efficient implementation of weighted ENO schemes*, J. Comput. Phys., **126**, 1996, pp.202–228.

[3] A. Majorana, R.M. Pidatella, *A finite difference scheme solving the Boltzmann-Poisson system for semiconductor devices*, to appear in J. Comput. Phys.

[4] C.-W. Shu, *Essentially non-oscillatory and weighted essentially non-oscillatory schemes for hyperbolic conservation laws*, in *Advanced Numerical Approximation of Nonlinear Hyperbolic Equations*, B. Cockburn, C. Johnson, C.-W. Shu and E. Tadmor (Editor: A. Quarteroni), Lecture Notes in Mathematics, volume 1697, Springer, 1998, pp.325-432.

List of Figures

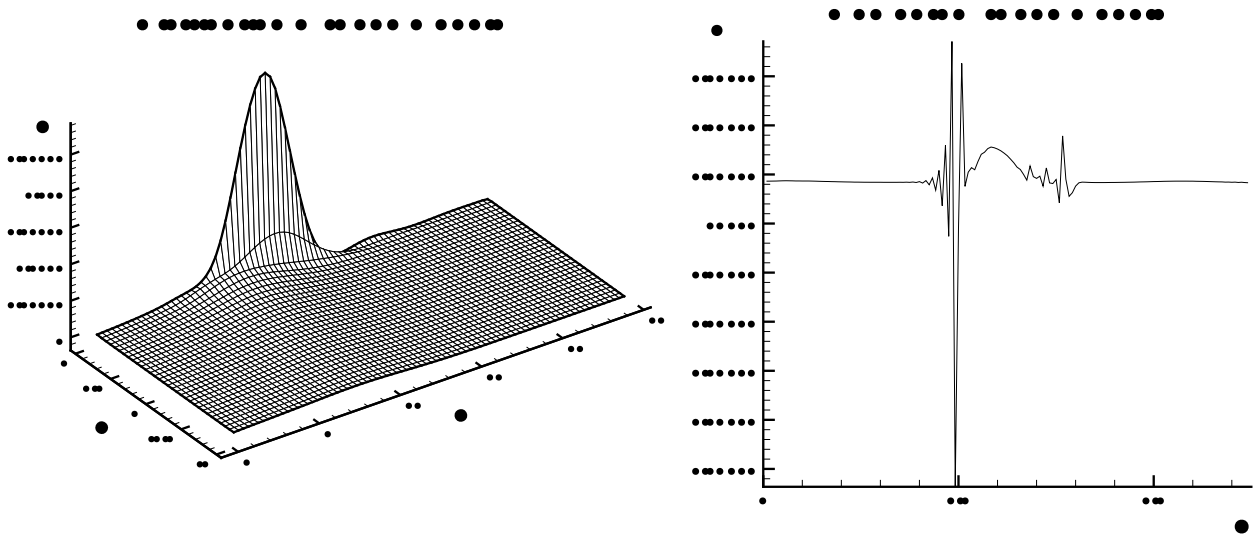

Figure 1: For the Kane model. Left: the stationary distribution function Φ, at the middle of the channel $z_0 = 0.125\mu m$; Right: the stabilization of the momentum.

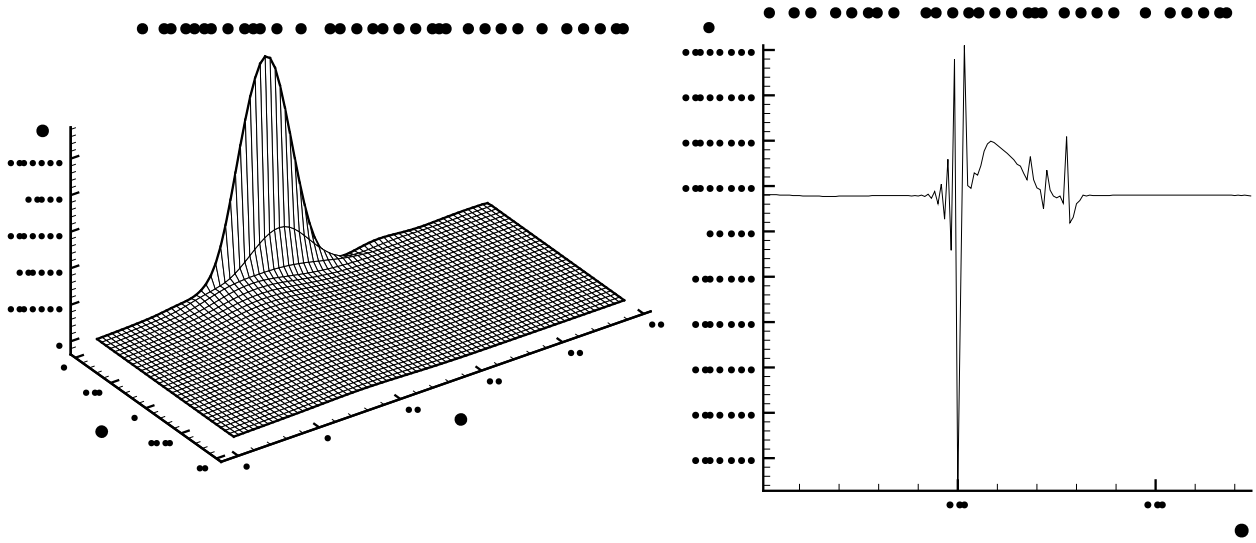

Figure 2: For the parabolic band model. Left: the stationary distribution function Φ, at the middle of the channel $z_0 = 0.125\mu m$; Right: the stabilization of the momentum.

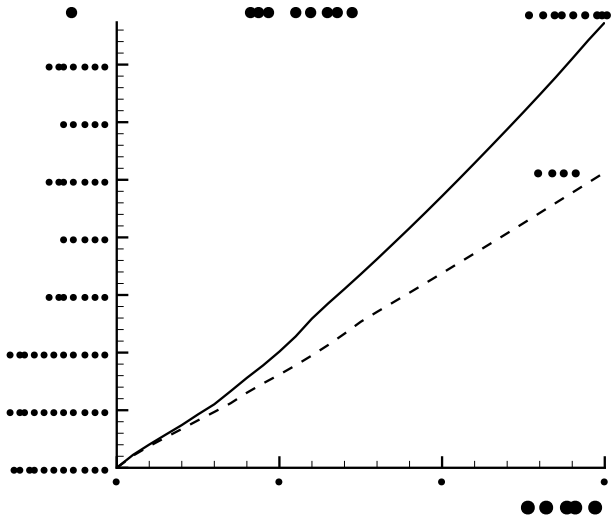

Figure 3: Comparison between the Kane and the parabolic band models for the Si n^+-n-n^+ 50 nm device. IV-curves (current I in $cm^{-2}sec^{-1}$ vs V_{bias} in Volt). Solid line: the parabolic band model; dashed line: the Kane model.

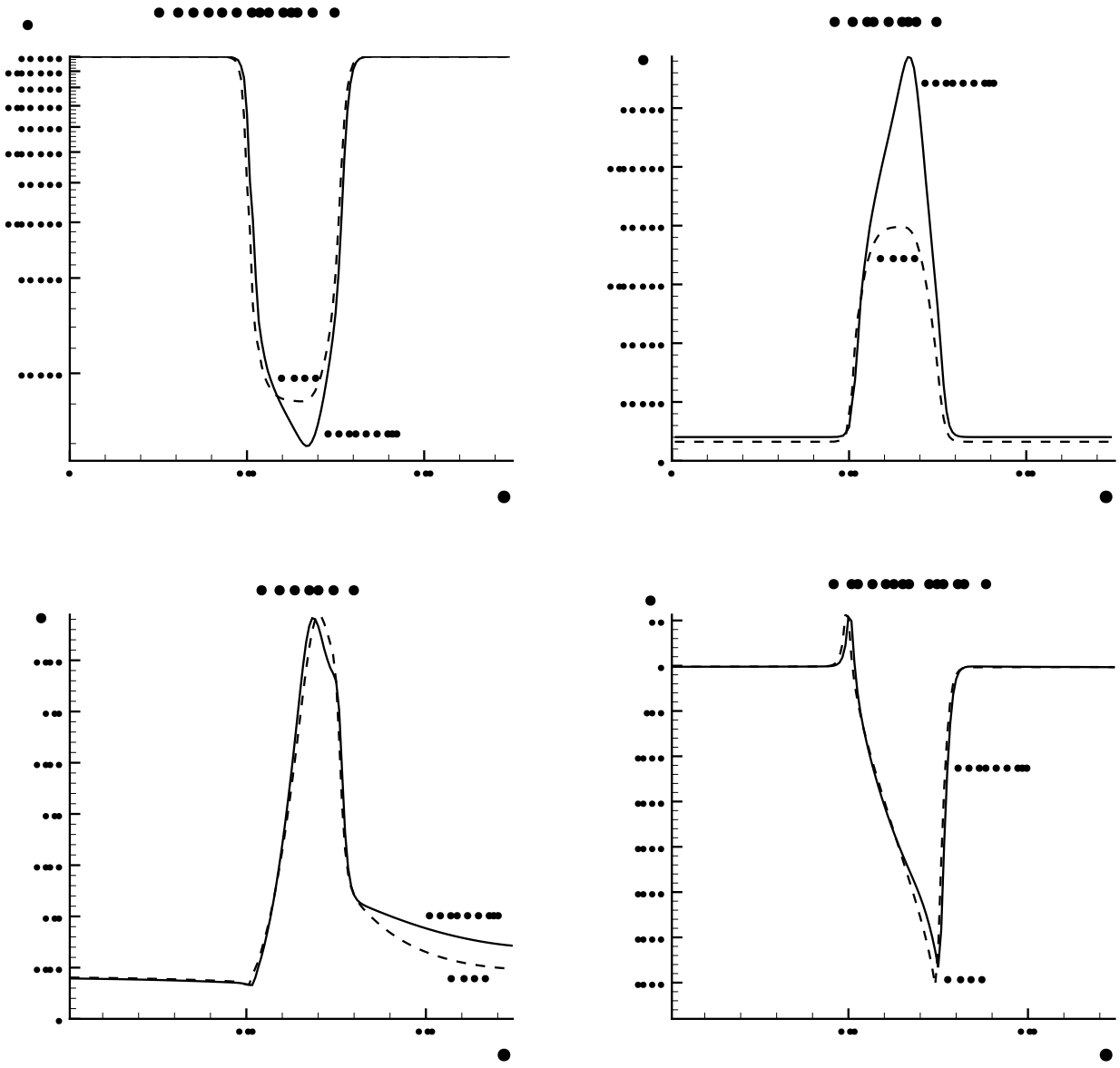

Figure 4: Comparison between the Kane and the parabolic band models for the Si n^+-n-n^+ 50 nm device at $V_{bias} = 1$V. Top left: the charge density n in cm^{-3}; top right: the (mean) velocity v in cm/sec; bottom left: the energy W in eV; bottom right: the electric field E in $10^3 V/cm$. Solid line: the parabolic band model; dashed line: the Kane model.